〈Original Papers〉 Continuous heavy precipitation with a winter occluding cyclone captured by GPM satellite in central Japan

Tsukuba Geoenvironmental Sciences, Vol. 15, pp. 1-11, Dec. 24, 2019

Continuous heavy precipitation with a winter occluding cyclone captured by GPM satellite in central Japan

Morihiro Sawada[a], Risa Anzai[b], and Kenichi Ueno[c]

Abstract

A fifth highest event of two-day accumulation precipitation in Honsyu area (Jan. 17-18, 2016) was nominated during the 10 winters since 2006 (Anzai and Ueno, 2018). Then, using Global Precipitation Measurement (GPM) dual-frequency precipitation radar (DPR) products, a case study was conducted to reveal the three-dimensional and synoptic scale structures of a precipitation system associated with a cyclone the mature stage. The disturbance in the front was composed of wide-ranging stratiform precipitation with a maximum of more than 2 km level by a poleward-ascending warm airstream moving over an easterly cold air mass. Subsequent convective precipitation was associated with an upper front due to dry intrusion over the warm conveyor belt. Successions of the stratiform to areas of convective precipitation were confirmed by surface weather radar images. We clarify that the combination of stratiform and convective precipitation was dependent on the conveyor belt structure of the cyclone toward the occluding stage and caused exceptional slow-moving heavy precipitation in central Japan.

Key words: heavy precipitation, Global Precipitation Mission, extratropical cyclone, occluding stage, central Japan

1. Introduction

Extremely heavy snow in the Kanto area in February 2014 caused various hazards, because an extratropical cyclone passed along the Pacific coast (the so-called South-coast cyclone, hereafter SCC). Mesoscale effects, such as cold-air damming (CAD), the formation of a coastal front, or side-feeder effects, have been considered to be key contributors to such heavy snowfalls (Fujibe, 1990; Araki, 2018; Kawase et al., 2018). To avoid damage to agriculture and housing or the occurrence of avalanches, mechanisms that increase the amount of total precipitation during the passage of a cyclone need to be determined. The large-scale topography of the Japanese archipelago primarily enhances the distribution of precipitation by the SCC (e.g., Ueno, 1989; Takano, 1996). Besides, Ando and Ueno (2015) showed that heavy precipitation in Honshu's inland tends to occur when the SCCs are in occlusion. The structure of the occluding cyclone associated with heavy precipitation areas has been introduced by the so-called conveyor belt model (Browning, 1997; Novak et al., 2008), which uses a combination of information regarding the warm conveyor belt (WCB), cold conveyor belt (CCB), and dry intrusion (DI). Schultz and Vaughan (2011) showed that dry air mass intrusion from the west in the occluding stage enhances the genesis of upper-level front and re-intensifies precipitation. Schemm and Wernli (2014) reported the intensification of the CCB due to the sensible heat of the WCB. Stratiform-convective transition within the WCB was also observed by NASA's A-Train satellite constellation (Crespo and Posselt, 2016). Kitabatake and Mitsui (1998) identified a split-type frontal system based on the model of Browning and Monk (1982) in Japan. However, the relationship between the synoptic scale precipitation fields characterized by a cyclone system and increased precipitation amounts has not been fully diagnosed around Japan as it has in the West. One reason is that precipitation radar on the ground does not effectively capture the three-dimensional structure of precipitation systems over complex topography, such as in Japan.

In 2014, the Global Precipitation Mission (GPM) core observatory (CO) started observing a three-dimensional precipitation field over Japan by dual-frequency precipitation radar (DPR) (Hou et al., 2014). This study took the opportunity to diagnose the synoptic-scale three-dimensional structure of the precipitation system associated with SCC that caused continuous wide-ranging heavy precipitation in southeastern central Japan. Based on the three-dimensional structure of the precipitation, we clarify the forming factor of the precipitation system and the relationship between it and airstreams with the cyclone.

2. Case study and data

From the winters of 2014-2017, a case of heavy precipitation on January 17-18, 2016 with GPM-CO observation was selected, when precipitation occurred widely

[a] Master's Program in Geoscience, Graduate School of Life and Environmental Sciences, University of Tsukuba, Tsukuba, Japan
[b] Japan Weather Association, Ikebukuro, Japan
[c] Faculty of Life and Environmental Sciences, University of Tsukuba, Tsukuba, Japan
(E-mail: ueno.kenichi.fw@u.tsukuba.ac.jp)

on the central Honshu Island, and heavy snowfall caused damage to communities in the Kanto-Koshinetsu area. According to 35 gauge measurements in central Japan (34°-38°N, east from 136°E), this ranked as the fifth highest two-day accumulation of precipitation in the previous 10 years (Anzai and Ueno, 2018). GPM-CO radar passed through the island of Honshu at 9:00 JST on January 18, crosscutting the cyclone system (Fig. 1 right, black lines), and comprehensively observing precipitation from Tokai to the Kanto and Tohoku areas (Fig. 1 right, pink, orange, and red lines, respectively).

The DPR is composed of Ku (13.8 GHz)- and Ka (35.5 GHz)-band precipitation radar (PR), hereafter KuPR and KaPR, respectively, where the KaPR (KuPR) is superior for detecting heavy precipitation (weak precipitation and precipitation phase discrimination) (JAXA, 2017b). This study used DPR level-2 products, including the radar reflectivity factor, precipitation rate, and melting layer detected by KuPR and KaPR (Iguchi et al., 2017). Radar scans the orthogonal cross section to the satellite pass with a width of 245 km and provides vertical and horizontal data with resolutions of 125 m and 5 km, respectively. The precipitation type, precipitation phase, and echo-level data (JAXA, 2017a) are also used to identify the mesoscale characteristics. The precipitation type includes three categories - stratiform, convective, and one other precipitation type - based on the horizontal and vertical characteristics of the radar reflectivity factor. The echo level is the height of the top KuPR-measured reflectivity factor. The synoptic condition was diagnosed using the Japanese 55-year Reanalysis (JRA-55), objective analysis data of the mesoscale model (MSM) (Saito et al., 2006), and water vapor channel data of the Multi-functional Transport Satellite-2 (MTSAT-2); temporal changes in the precipitation distribution were captured by Japan Meteorological Agency (JMA) operational (composite) weather radar images and JMA Automated Meteorological Data Acquisition System (AMeDAS) gauge data. The airflow system in the cyclone was identified by JMA radio sounding (RS) and wind profiler (WP) data.

3. Synoptic scale condition and airflow system

According to the conveyor-belt model (Browning, 1997; Catto et al., 2010), the WCB provides rich water vapor ascending along cold fronts or over warm fronts in the warm sector, and it splits toward the cyclone center anticlockwise or overshoots ahead of the cyclone system. The CCB moves ahead the southwest of cyclone center at a low level, and the head is sometimes associated with a sting-jet storm (Hart et al., 2017). DI prevails at the upper level behind the surface cold front and is seen as an anticlockwise spiral dry slot toward the cyclone center in the water vapor image (James and Clark, 2003). Those features were referenced to diagnose the synoptic scale airflow system of the target case.

The target SCC brought extremely heavy rains to

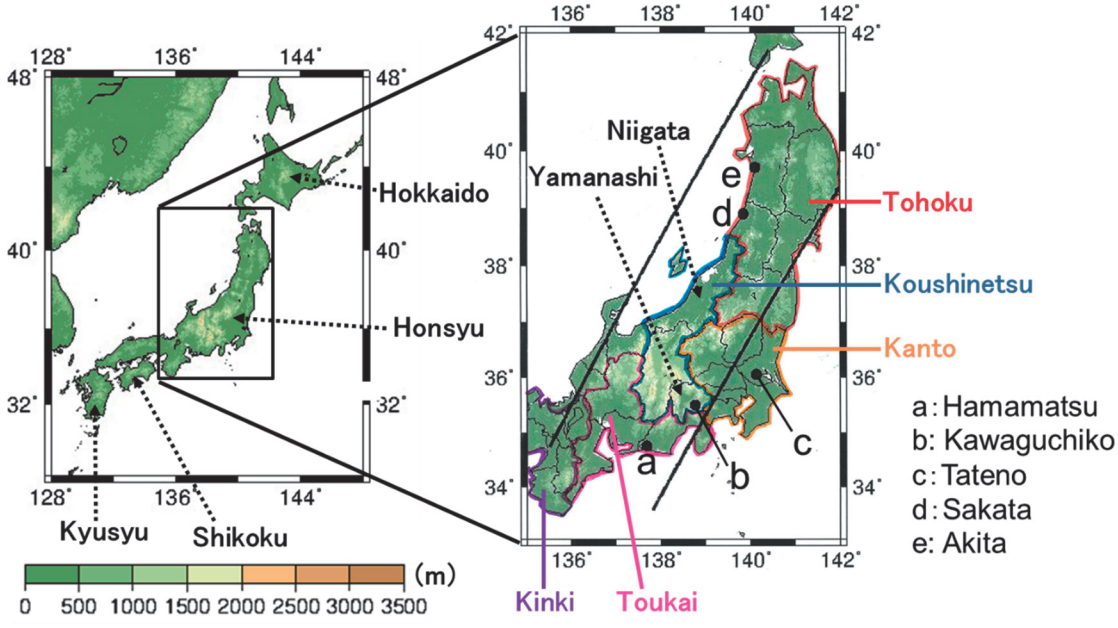

Fig. 1 Topography of Japan with major aerial divisions and radio sounding and wind profiler observatories, including Hamamatsu (a), Kawaguchiko (b), Tateo (c), Sakata (d), and Akita (e). The GPM-CO observation area is between the black lines.

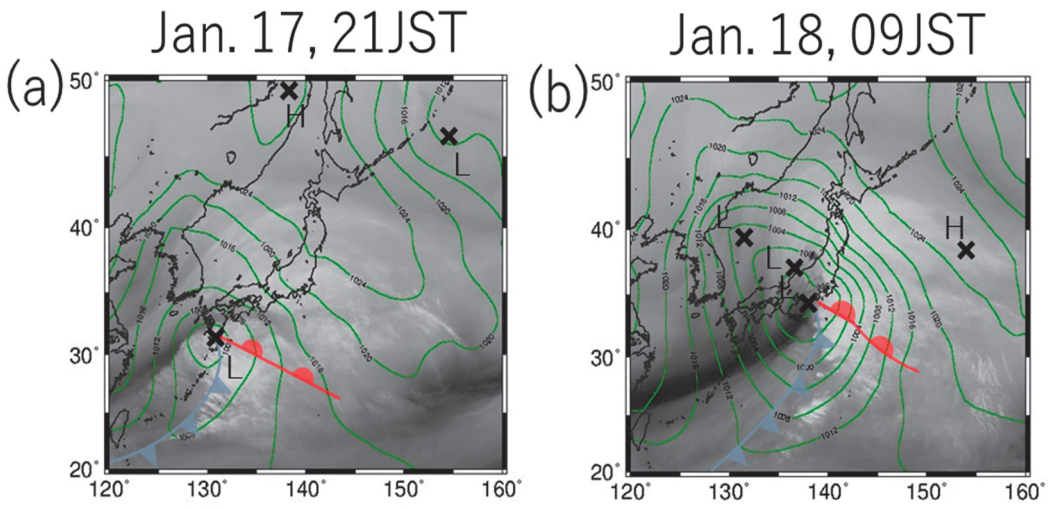

Fig. 2 (a) Sea-level pressure with surface fronts quoted by JMA's surface weather maps and low (high) pressure systems and moisture image on January 17, 21:00 JST. The same for (b) on January 18, 9:00 JST.

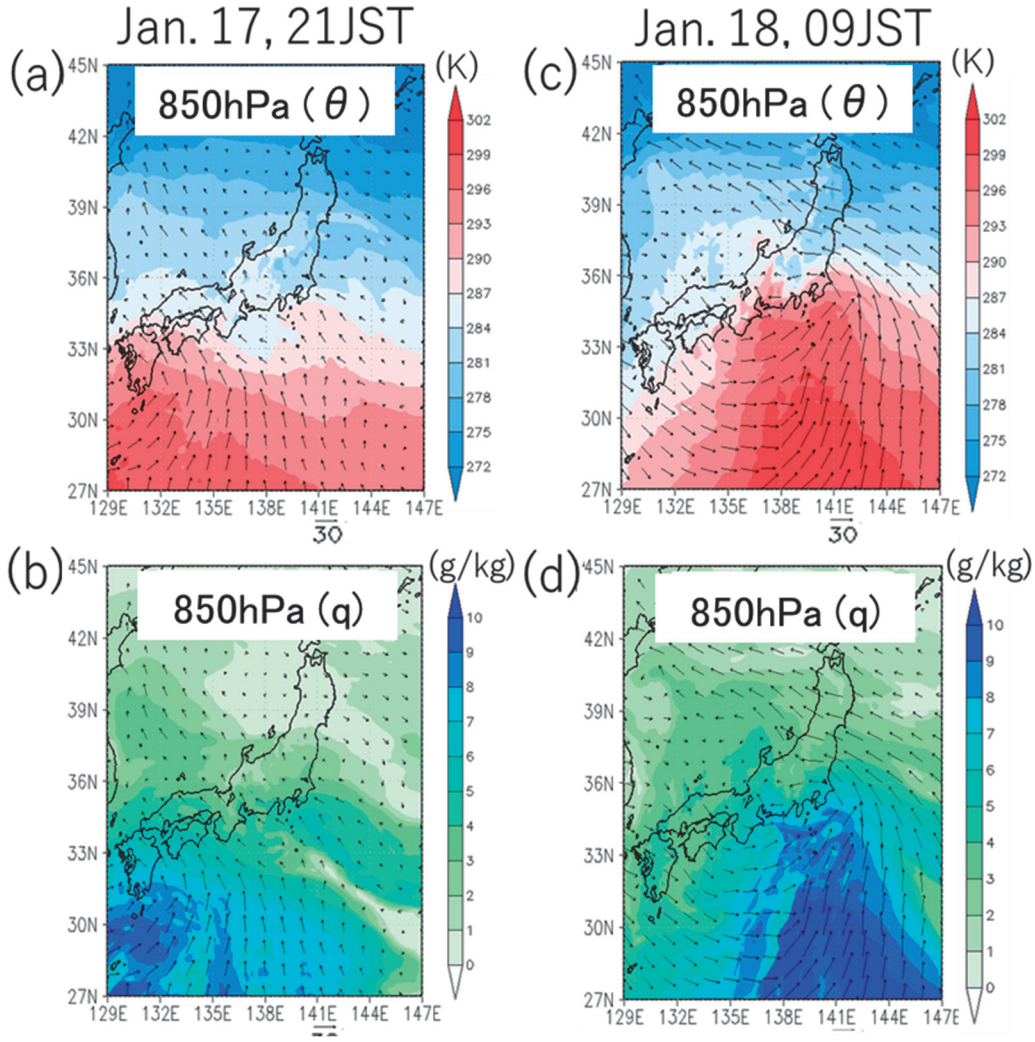

Fig. 3 (a) Potential temperature (θ) with wind vector at 850 hPa, and (b) specific humidity (q) with wind vector at 850 hPa on January 17, 21:00 JST. The same for (c), (d) on January 18, 9:00 JST.

Okinawa and approached southern Kyushu island on January 17. On January 18, three cyclone centers were analyzed around central Japan, and heavy precipitation occurred in the Kanto area. At 21:00 JST on January 17, the cyclone center of 1000 hPa was located in south Kyushu when wide-ranging clouds already covered Honshu. A dry zone indicated that DI ran from the southwest far behind the surface cold front and curved eastward north of the cyclone center (Fig. 2a). In front of the cyclone system, the sea-level pressure distribution showed that the high-pressure area extended southeastward over the northwestern Pacific, causing cold easterlies as the CCB moved to the Tohoku area (Fig. 3a). A small pressure trough over the central mountain range in Tohoku and central Japan was also analyzed, which indicated the occurrence of cold-air damming. Around the cyclone center, low-level (850 hPa) potential temperature and specific humidity indicated warm and moisture currents toward the north as a WCB (Fig. 3a,b), and they became clearer on the morning of January 18. At the mid-level (500 hPa), the currents intruded over the surface warm front into western Japan; however, DI was not analyzed at this level (Fig. 4a,b).

At 9:00 JST on January 18, the DI split over the east of Kyushu Island, and the eastward branch caused multiple tall convections aligned from the coastal area to the Pacific (Fig. 2b). The SCC lowered the central pressure to 988 hPa, with two other low-pressure centers in the north. A surface pressure ridge in the northeast caused by high pressure with a center of 1024 hPa was strengthened, and a stronger pressure gradient intensified the easterly CCB into the Tohoku area (shown later). Warm currents, at 850 hPa from the southwest, were staged by the easterly cold current at around 36°N, and cold currents prevailed in

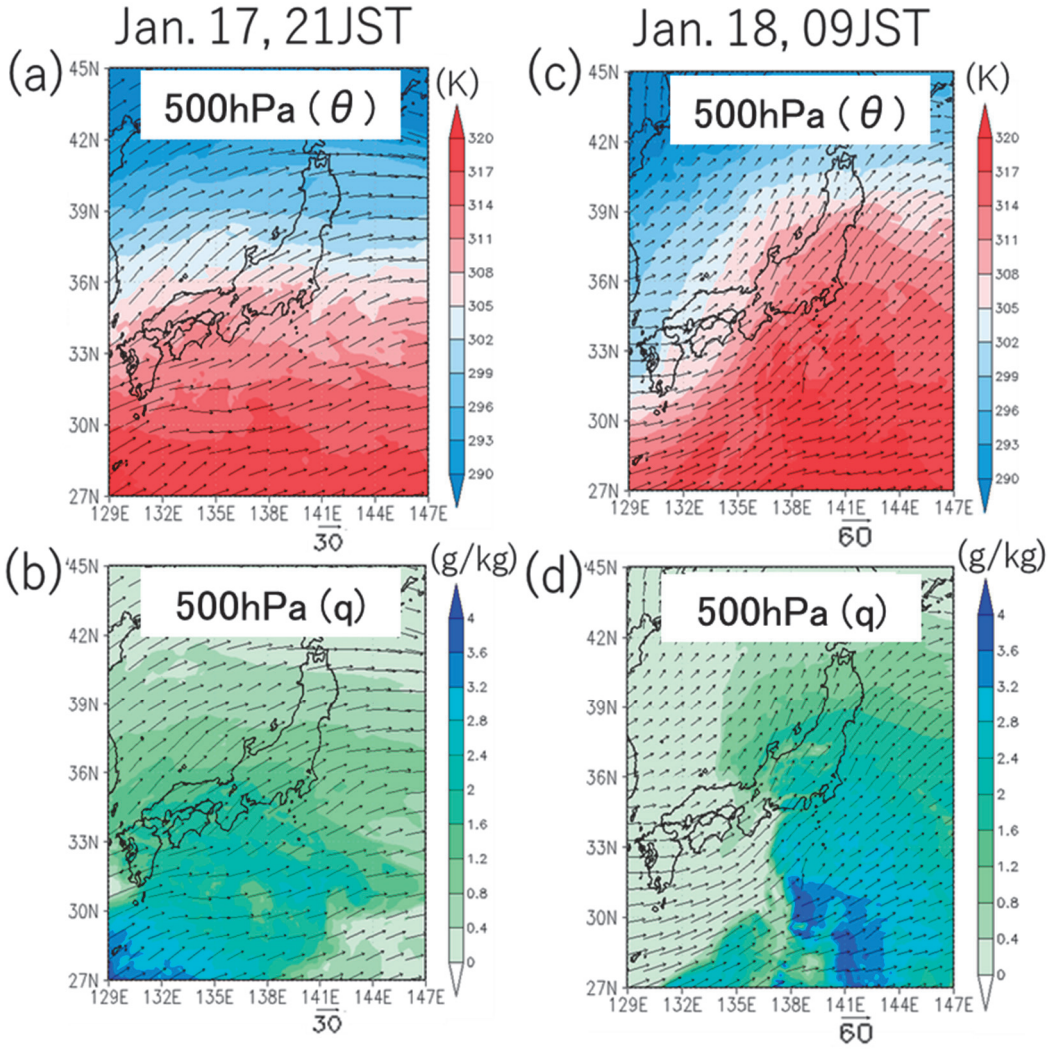

Fig. 4 (a) Potential temperature with wind vector at 500 hPa, and (b) specific humidity with wind vector at 500 hPa on January 17, 21:00 JST. The same for (c) - (d) on January 18, 9:00 JST.

central Japan (Fig. 3c). Additionally, wide areas of rich moisture more than 10 g/kg dominated south of 31°N but did not reach the coasts (Fig. 3d), indicating that atmospheric river-like moisture intrusion was not the major cause of heavy precipitation over land. At the mid-level, southwesterly warm and moistened current flowed over the CCB and intruded into eastern Japan (Fig. 4c, d). Upper-level dry intrusion around the cyclone center over the strong low-level anticlockwise flow with a mid-level warm southwesterly resembles the occluding stage of a cyclone as described by Schultz and Vaughan (2011). Actually at 21:00 JST on January 18, an occluded front was analyzed in the JMA surface weather chart, and the cyclone intensified and moved northeastward along the east coast (figure omitted).

Next, vertical structures of the wind shear and instability associated with major conveyor belts were analyzed using the RS and WP data at 9:00 JST on January 18.

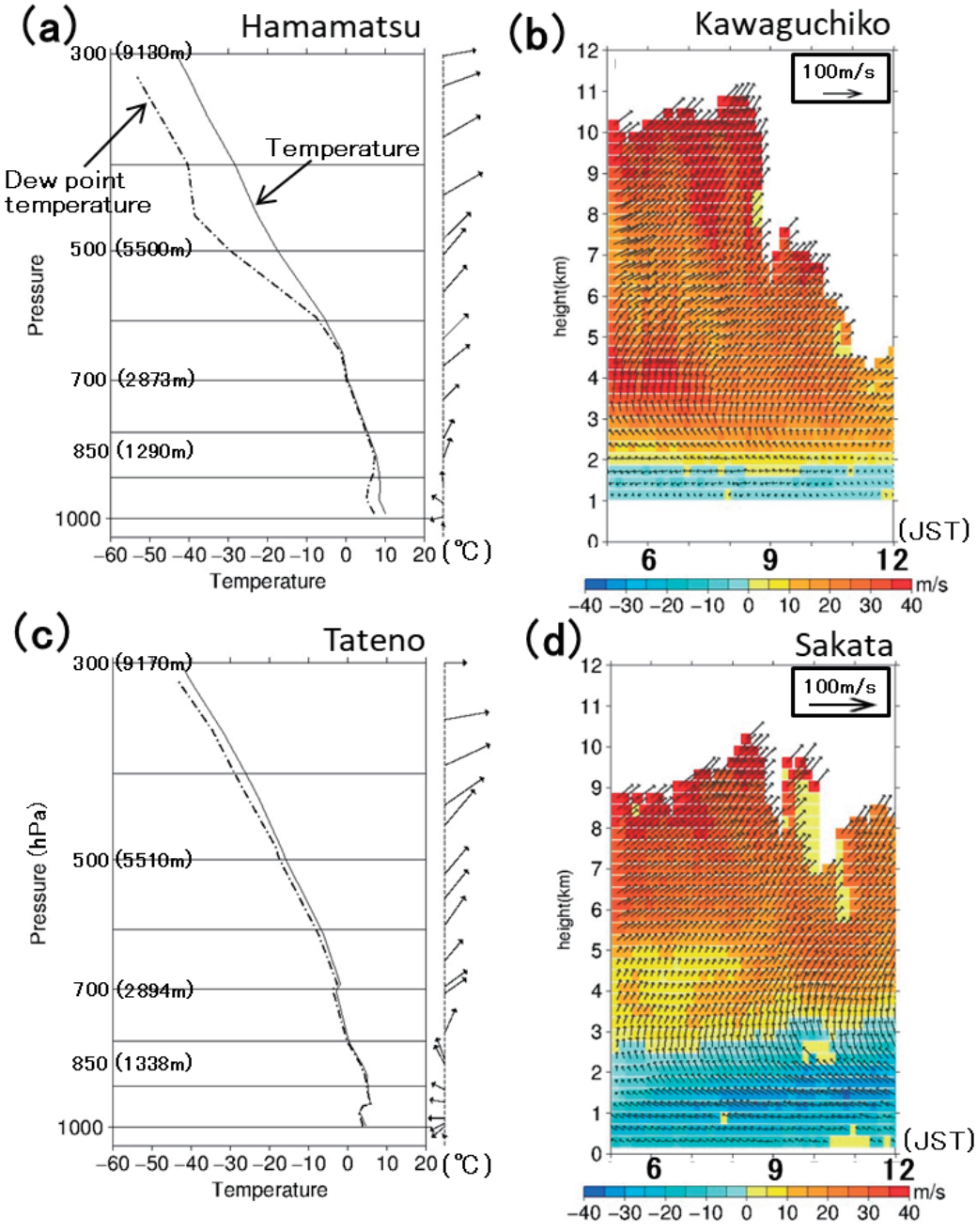

Fig. 5 Temperature, dewpoint temperature, and wind vector profiles at (a) Hamamatsu and (c) Tateno, at 9:00 JST on January 18, 2016. Wind profile changes at (b) Kawaguchiko and (d) Sakata on January 18.

The RS profile at Hamamatsu showed that an unsaturated easterly cold air flow prevailed below 900 hPa and a moistened southwesterly prevailed above until 600 hPa (Fig. 5a), indicating that the WCB was intruding along the Pacific coast over the low-level CCB as shown in Fig. 4c, d. Above 600 hPa, a large difference between the dewpoint temperature and the temperature indicates DI, which is clearly seen in the water vapor image (Fig. 2b). The WP observation at Kawaguchiko (860 m above sea level) showed a similar structure, such as a weak easterly below the 2 km level and a south to a southwesterly up to 10 km from the ground. The height of the southerly upper winds suddenly decreased to 7 km after 9 a.m. and then lower still after 11 a.m., indicating that DI disturbed the upper-level wind detection by the WP. According to the RS profile at Tateno northeast of Kanto (Fig. 5c), a low-level easterly flow (CCB) was thicker than that of Hamamatsu until 850 hPa, and a shallow cold inversion layer existed in the easterly at 950 hPa. The southwesterly flow above was moistened, and DI was not identified (that agrees with the satellite image in Fig. 2b). WP data at Sakata and the west coastal points of Tohoku showed that low-level easterly winds became thicker and stronger on the morning of January 18, indicating the development of the CCB ahead of the cyclone center, with intensification of a stagnant pressure ridge to the northeast.

4. Temporal changes in precipitation

The two-day accumulated precipitation distribution for January 17–18 (Fig. 6a) showed that a zonal precipitation maximum extended in the east-west direction from southern Yamanashi Prefecture toward Kanto, and another maximum zone appeared along the eastern Pacific coast. According to the time sequences of hourly precipitation at three stations (Fig. 6b), precipitation started on the night of January 17 in the Koshinetsu area, with gradually increasing amounts, peaking at around 9:00 JST on January 18, when the GPM-CO passed. Hourly precipitation rates continued to increase in the Kanto area, particularly on the east coast, including Choshi, and continued until afternoon. Snow accumulated in inland areas with higher elevations, such as at Kawaguchiko, from midnight on January 17 until morning on January 18. Several centimeters of snow also fell in Tokyo in the early morning, causing traffic problems. The high-ranking accumulated precipitation in this case was not due to the short-term extreme precipitation but rather to the continuation of moderate precipitation for more than half a day.

Temporal changes of the spatial precipitation distribution from 21:00 JST on January 17 to 12:00 JST on January 18 were examined by JMA radar images (Fig. 7). Stratified precipitation areas intruded from western Japan, as shown in Fig. 7a, and spread over central Japan in the middle of the night (Fig. 7b) with weak intensity of less than 3 mm/h. Then, after the intrusion of spotty precipitation-free areas, zonal convective precipitation bands with the intensity of more than 10 mm/h intruded from the Pacific side toward the northeast (Fig. 7c, marked X). This precipitation band prevailed with an eastward motion around the Tokai area. Besides, in Kanto, a circle, show-

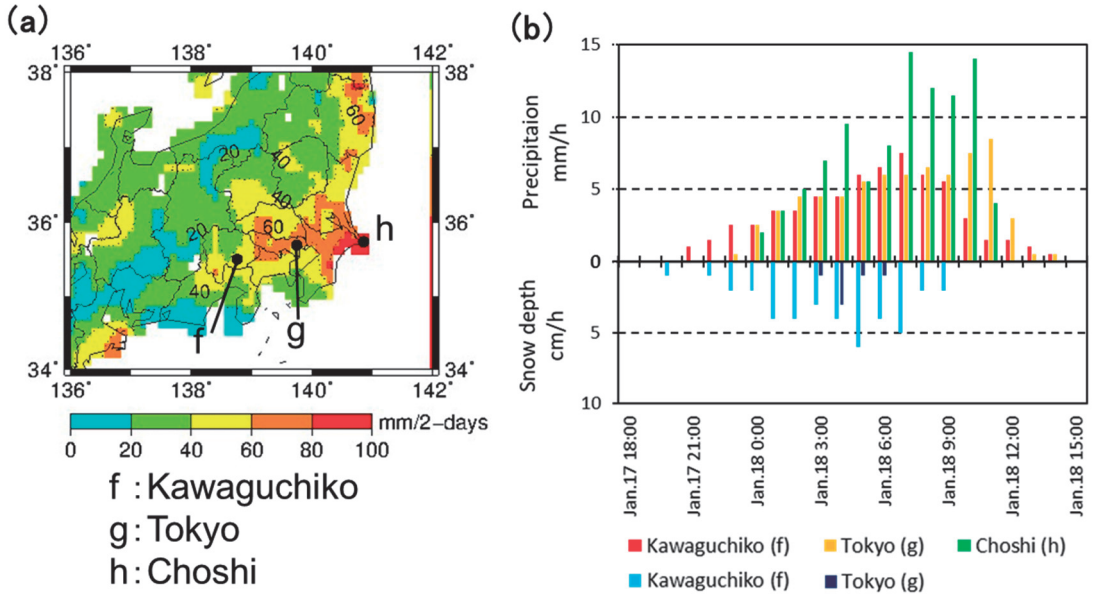

Fig. 6 (a) Accumulated precipitation for January 17-18 in central Japan, and (b) hourly precipitation and snow depth changes at major spots of heavy precipitation in Japan Standard Time.

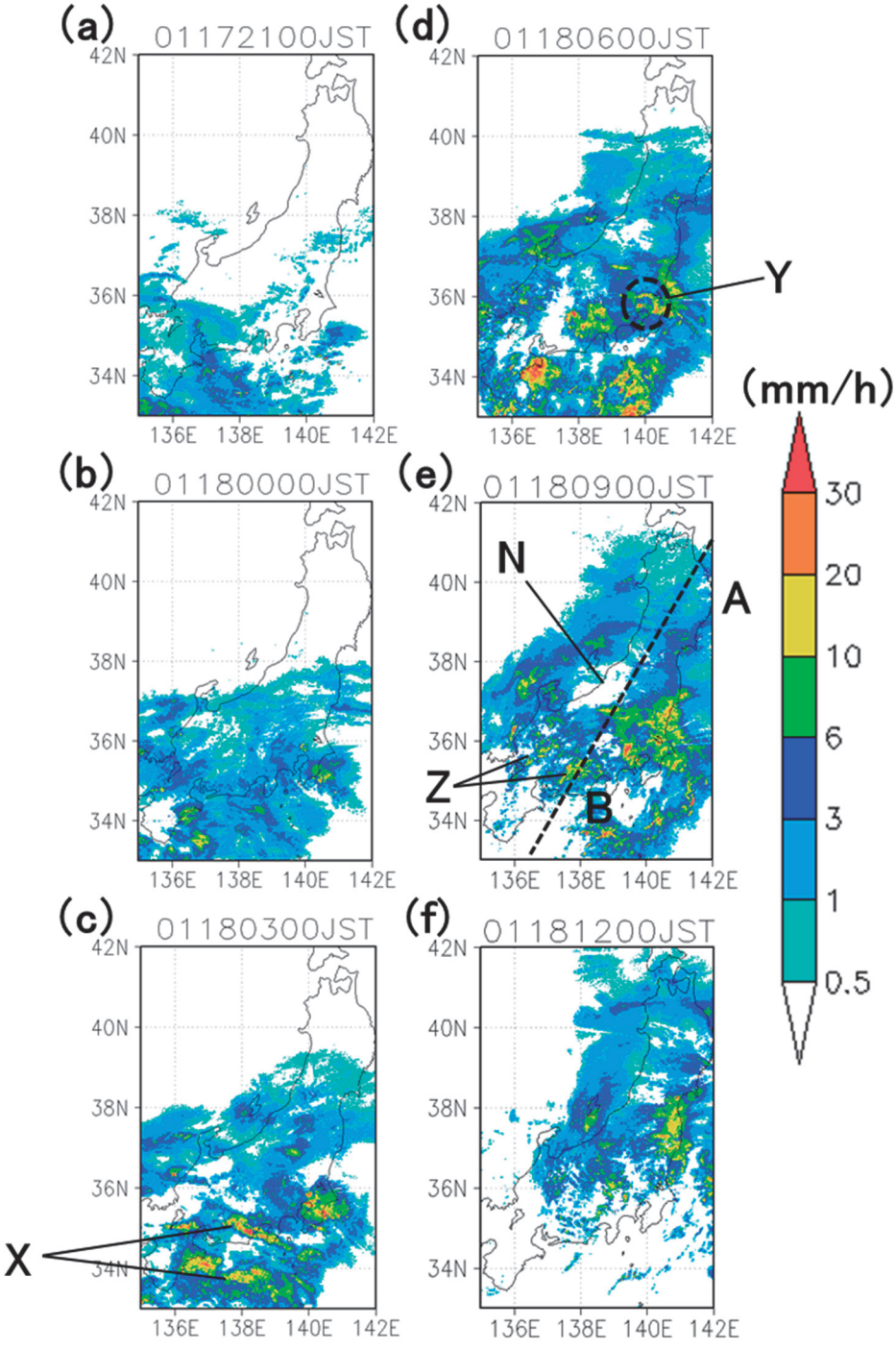

Fig. 7 Three-hourly JMA weather radar echoes, starting from 21:00 JST on January 17 (a) until 12:00 JST on January 18 (f).

ing as bright bands due to the melting of snow, sometimes appeared on the radar image (Fig. 7d, marked Y), indicating that stratified precipitation with melting layers contributed to the early morning precipitation there. Such preceding stratified precipitation areas extended over the Tohoku area at 9:00 JST on January 18 (Fig. 7e, marked A), with precipitation-free areas behind (Fig. 7e, N), around Niigata Prefecture. At the same time, convective rain areas still prevailed in the southeast (marked B), causing another precipitation increase on the Kanto plain. As the SCC developed and moved rapidly northeastward (Fig. 7f), convective heavy precipitation near the cyclone

center caused another heavy coastal precipitation zone, as shown in Fig. 6a. Namely, continuous precipitation from January 17 to 18 was caused by widespread stratiform clouds (area A) in the first half, and successive intensive convective clouds (area B) embedded in the target SCC.

5. Precipitation types and cyclone organization

Figure 8 shows a vertical cross section of DPR-KuPR echo intensity at 9:00 JST on January 18 along a dashed line in Fig. 7e, with the precipitation type and echo-top height distribution by the DPR products in the areas between the black lines of Fig. 1. The vertical section (Fig. 8a) clearly shows that the cyclone was composed of (1) stratiform echoes with a maximum of more than 2 km over area A, and (2) convective echoes with low-level maximums below 4 km over area B, with sandwiched precipitation-free areas corresponding to mark N in Fig. 8e. In area A, the echo-top height increased up to 6 km while going south in the cross section corresponding to the DPR product (Fig. 8c), where the bottom of the echo profile vanished (maybe evaporated), as marked P in Fig. 8a, where the precipitation type of the DPR product was categorized as "other" (Fig. 8b). In area B, multiple strong low-level echoes were identified over the central mountains, and the DPR products of Fig. 8b also produced several convective spots. However, the echo-top height was not as extremely high as that of summer cumulonimbi, which reached the troposphere. In the distribution of echo-top height, longitudinal zonal structure was found (Fig. 8c, marked Q). The bands were also found on the JMA radar image (Fig. 7e, marked Z).

According to the organization of the cyclone as diagnosed in Chapter 3, the stratiform precipitation maximum zone in area A corresponded to the layer above the strong wind shear due to WCB intrusion over the CCB ahead of the cyclone system. According to the potential temperature profile at Akita (cross marks in Fig. 9), obvious convective instability was not detected. In area B, a strong layer of convective instability was found in the 500-650 hPa layer at Hamamatsu (black circles in Fig. 9), due to dry intrusion over the moist WCB. The longitudinal zonal structure in the echo-top distribution (Fig. 8c, marked Q) was embedded in the DI and aligned with the upper-level wind direction. Therefore, we concluded that the upper front structure by DI over the WCB could contribute to the formation of convective precipitation areas following the eastward movement of SCC in the mature stage.

6. Conclusions

A winter SCC that provided wide-ranging heavy precipitation in central Japan on January 17-18, 2016, was diagnosed by state-of-the-arts products of GPM-DPR with multiple surface observations and reanalysis data. Stratiform precipitation was caused in the first half of the cyclone event at a level over 2000 m, due to the WCB's ascending over the CCB with a strong wind shear, and the following convective precipitation was associated with the upper front, due to a convergence of upper DI over the WCB with convective instability. Two successive type of precipitation, such as stratiform and convective precipitation, at the mature stage of the cyclone caused a heavy precipitation zone from Yamanashi Prefecture to eastern Kanto. GPM-DPR observation can capture the precipitation structure on a synoptic scale at once in the complex archipelago, and we clarify the relationship of the cyclone with precipitation systems and airstreams.

According to Ueno et al. (2019), severe overestimation in the data of the Global Satellite Mapping of Precipitation (GSMaP, Kubota et al. 2007) associated with extratropical cyclones was found. We speculate that wide-ranged high-level stratiform precipitation as found in this case study may enhance the scattering microwave signals. Further GPM-DPR data accumulation is anticipated to increase more case studies and diagnose three-dimensional precipitation systems in accordance with the different development stages of the SCCs. For instance, extreme heavy rains in Chiba prefecture on Oct. 25, 2019, was also caused by an extratropical cyclone associated with clear DI, humid low-level intrusion from the south, and stagged by a Typhon No. 21 in front. GPM-DPR observed some parts of the heavy rain areas and further analysis is anticipated.

Acknowledgments

We used MTSAT-2 data received by the JMA, Weathernews Inc., and Takeuchi Lab; given to the Earthquake Research Institute and Institute of Environment Science, University of Tokyo; and processed and released by the Center for Environmental Remote Sensing, Chiba University. This research was supported by the second Research Announcement on the Earth Observations of Japan Aerospace Exploration Agency (JAXA). The authors are grateful to Dr. M. Yamamoto (JAXA-EORC) and Mr. Mito and Mr. Yokoyama (University of Tsukuba) for their help in data resampling and their constructive comments.

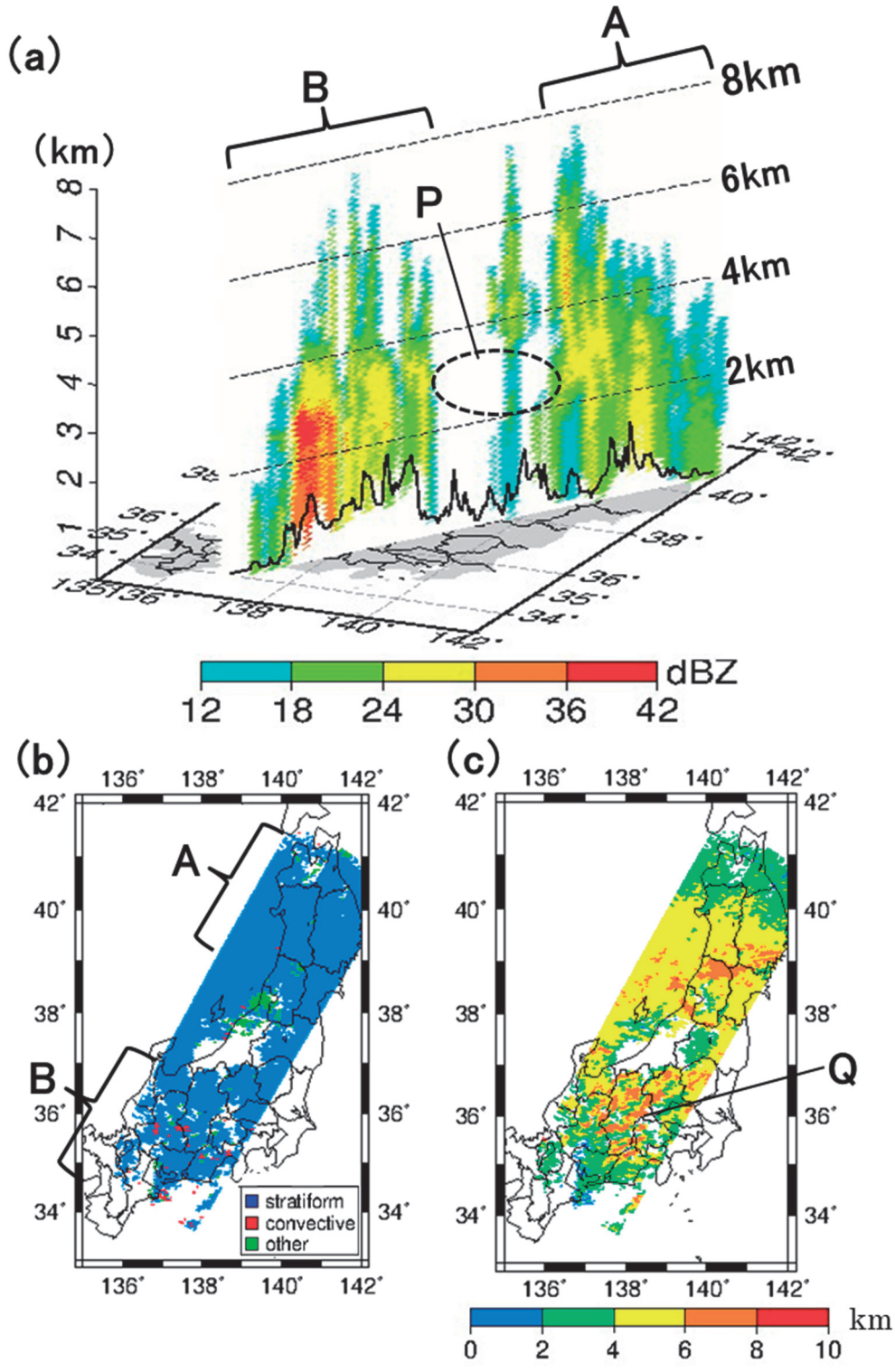

Fig. 8 (a) Vertical cross section of DPR KuPR echo, (b) precipitation type distribution, and (c) echo-top height distribution at 9:00 JST on January 18.

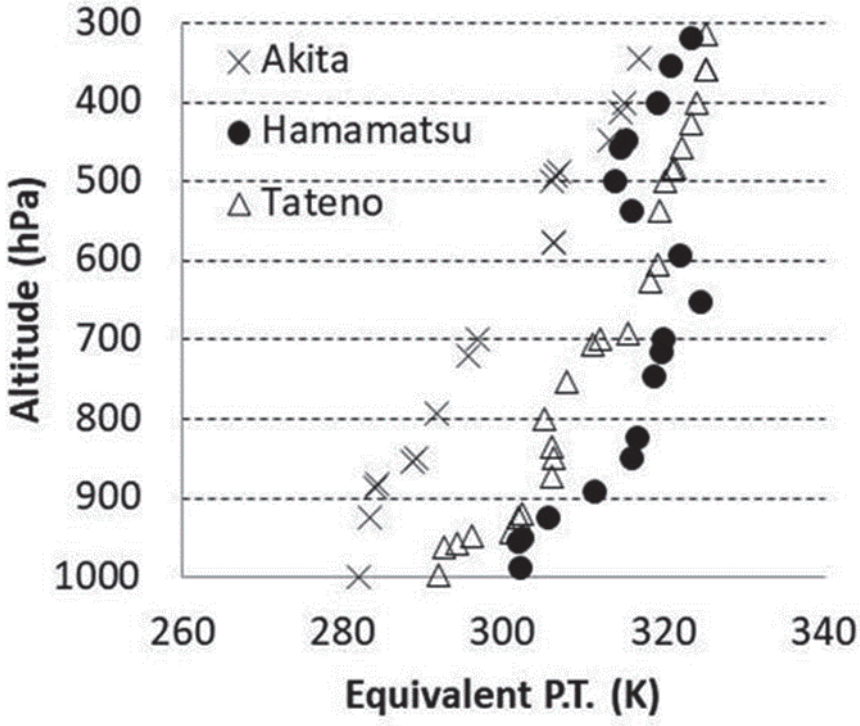

Fig. 9 Profiles of equivalent potential temperatures at 9:00 JST on January 18 at Akita (×), Hamamatsu (●), and Tateno (△).

References

Ando, N., and Ueno, K. (2015): Occurrence tendency of heavy rainfall or snowfall in the inland district of Japan in winter. *Seppyo*, **77**, 397-410 (in Japanese). http://www.geoenv.tsukuba.ac.jp/~kueno/Ando2015.pdf

Anzai, R., and Ueno, K. (2018): Occluding winter extratropical cyclone with heavy precipitation. *Abstract of MSJ 2018 Spring Meeting*, 184 (in Japanese).

Araki, K. (2018): Snowfall characteristics of heavy snowfall events associated with cyclones causing surface avalanche in Nasu, Japan. *Seppyo*, **80**, 131-147 (in Japanese). http://www.bosai.go.jp/seppyo/kenkyu_naiyou/nasu/NasuKakenReport_chapter3-3.pdf

Browning, K. A., and Monk, G. A. (1982): A simple model for the synoptic analysis of cold fronts. *Quarterly Journal of the Royal Meteorological Society*, **108**, 435-452. https://rmets.onlinelibrary.wiley.com/doi/10.1002/qj.49710845609

Browning, K. A. (1997): The dry intrusion perspective of extratropical cyclone development. *Meteorological Applications*, **4**, 317–324. https://rmets.onlinelibrary.wiley.com/doi/abs/10.1017/S1350482797000613

Catto, J. L., Shaffrey, L. C., and Hodges, K. I. (2010): Can climate models capture the structure of extratropical cyclones? *Journal of Climate*, **23**, 1621-1635. https://journals.ametsoc.org/doi/10.1175/2009JCLI3318.1

Crespo, J.A., and Posselt, D. J. (2016): A-Train-based case study of stratiform-convective transition within a warm conveyor belt. *Monthly Weather Review*, **144**, 2069-2084. https://journals.ametsoc.org/doi/full/10.1175/MWR-D-15-0435.1

Fujibe, F. (1990): Climatology of the coastal front in the Kanto Plain. *Papers in Meteorology and Geophysics*, **41**, 105-128. https://www.jstage.jst.go.jp/article/mripapers/41/3/41_3_105/_article/

Hart, N. C. G., Gray, S. L., and Clark, P. A. (2017): Sting-jet windstorms over the North Atlantic: Climatology and contributions to extreme wind risk. *Journal of Climate*, **30**, 5455-5471. https://journals.ametsoc.org/doi/10.1175/JCLI-D-16-0791.1

Hou, A. Y., Kakar, R. K., Neeck, S., Azarbarzin, A. A., Kummerow, C. D., Kojima, M., Oki, R., Nakamura, K., and Iguchi, T. (2014): The global precipitation measurement mission. *Bulletin of the American Meteorological Society*, **95**, 701-722. https://journals.ametsoc.org/doi/10.1175/BAMS-D-13-00164.1

Iguchi, T., Seto, S., Meneghini, R., Yoshida, N., Awaka, J., Le, M., Chandrasekar, V., and Kubota, T. (2017):

GPM/DPR level-2 algorithm theoretical basis document, Volume 3, 15 (Available online at http://www.eorc.jaxa.jp/GPM/doc/algorithm/ATBD_DPR_201708_whole_1.pdf, accessed June 20, 2018).

James, R. P., and Clerk, J. H. E. (2003): The diagnosis of vertical motion Within dry intrusions. *Weather and Forecasting*, **18**, 825-835. https://journals.ametsoc.org/doi/full/10.1175/2007MWR2111.1

JAXA (2017a): GPM/DPR L2/3 product format documentation version 3.2, Volume 2, 40-50 (Available online at https://journals.ametsoc.org/doi/full/10.1175/2007MWR2111.1, accessed June 20, 2018).

JAXA (2017b): Overview of GPM products version 2.1, Volume 1. 11 (Available online at https://journals.ametsoc.org/doi/full/10.1175/2007MWR2111.1, accessed June 20, 2018)

Kawase, H., Sasai, T., Yamazaki, T., Ito, R., Dairaku, K., Sugimoto, S., Sasaki, H., Murata, A. and Nosaka, M. (2018): Characteristics of synoptic conditions for heavy snowfall in western to northeastern Japan analyzed by the 5-km regional climate ensemble experiments. *Journal of the Meteorological Society of Japan*, **96**, 161-178. https://journals.ametsoc.org/doi/full/10.1175/2007MWR2111.1

Kitabatake, N., and Mitsui, K. (1998): Synoptic analysis of extratropical cyclones with the split front system. *Tenki*, **45**, 33-43 (in Japanese). https://journals.ametsoc.org/doi/full/10.1175/2007MWR2111.1

Kubota, T., Shige, S., Hashizume, H., Aonashi, K., Takahashi, N., Seto, S., Hirose, M., Takayabu, Y. N., Nakagawa, K., Iwanami, K., Ushio, T., Kachi, M., and Okamoto, K. (2007): Global precipitation map using satellite borne microwave radiometers by the GSMaP Project: Production and validation. *IEEE Transactions on Geoscience and Remote Sensing*, **45**, 2259-2275.

Novak, D. R., Colle, B. A., and Yuter, S. E. (2008): High-resolution observations and model simulations of the life cycle of an intense mesoscale snowband over the northeastern United States. *Monthly Weather Review*, **136**, 1433-1456. https://journals.ametsoc.org/doi/10.1175/2007MWR2233.1

Saito, K., Fujita, T., Yamada, Y., Ishida, J., Kumagai, Y., Aranami, K., Ohmori, S., Nagasawa, R., Kumagai, S., Muroi, C., Kato, T., Eito, H., and Yamazaki, Y. (2006): The operational JMA nonhydrostatic mesoscale model. *Monthly Weather Review*, **134**, 1266-1298. https://journals.ametsoc.org/doi/10.1175/MWR3120.1

Schemm, S., and Wernli, H. (2014): The linkage between the warm and the cold conveyor belts in an idealized extratropical cyclone. *Journal of the Atmospheric Sciences*, **71**, 1443-1459. https://journals.ametsoc.org/doi/10.1175/JAS-D-13-0177.1

Schultz, D. M., and Vaughan, G. (2011): Occluded fronts and the occlusion process: A fresh look at conventional wisdom. *Bulletin of the American Meteorological Society*, **92**, 443-466. https://journals.ametsoc.org/doi/abs/10.1175/2010BAMS3057.1

Takano, I. (1996): Numerical simulations of an orographically-induced mesoscale cloud system and subsequent cyclogenesis off the south coast of Japan. *Journal of the Meteorological Society of Japan. Ser. II*, **74**, 673-694. https://doi.org/10.2151/jmsj1965.74.5_673

Ueno. K. (1989): Relations between changes of hourly precipitation distribution and topography during an extratropical cyclone passing over Japan. *Chirigakuhyoron*, **62A**(11), 776-791 (in Japanese). https://www.researchgate.net/publication/291268990

Ueno, K., Mito, W., Kanai, R., Ueji, Y., Suzuki, K., Kobayashi, H., Tamagawa, I., Yamamoto, M.K. and Shige, S. (2019): Distribution of precipitation depending on synoptic scale disturbances with satellite estimate comparisons in the Japanese Alps area during warm seasons. *Journal of Geography (Chigaku Zasshi)*, **129**, 31-47 (in Japanese with an English abstract).